Hydrogen plasma treated nanodiamonds lead to an overproduction of hydroxyl radicals and solvated electrons in solution under ionizing radiation

Emilie Brun, Hugues Girard, Jean-Charles Arnault, Michel Mermoux, Cécile Sicard-Roselli

Hydrogen plasma treated nanodiamonds lead to an overproduction of hydroxyl radicals and solvated electrons in solution under ionizing radiation

Emilie Brun*[a], Hugues A. Girard[b], Jean-Charles Arnault[b], Michel Mermoux[c], Cécile Sicard-Roselli[a]

a. Institut de Chimie Physique UMR 8000, CNRS, Université Paris-Saclay, Orsay, F-91405, France

b. CEA, LIST, Diamond Sensors Laboratory, F-91191 Gif-sur-Yvette, France

c. Univ. Grenoble Alpes, Univ. Savoie Mont Blanc, CNRS, Grenoble INP, LEPMI, 38000 Grenoble, France

*Corresponding author: Tel: (33) 1 69 15 42 74 emilie.brun@universite-paris-saclay.fr

Abstract

In numerous fields of application (environmental remediation, catalysis, nanomedicine), production of hydroxyl radicals and solvated electrons by nanomaterials is a cornerstone. Through a very sensitive, nanoparticle-compatible, coumarin-based protocol, we quantified hydroxyl radicals in solution when hydrogenated (H-ND) and oxidized (Ox-ND) detonation nanodiamonds were irradiated by MeV photons. We highlighted a blatant difference between the two surface chemistries as only H-ND led to 50% more radicals, for irradiation doses and ND concentrations relevant in nanomedicine. For the first time, we also quantified solvated electrons after keV irradiation of both suspensions and showed that in the presence of H-ND, hydroxyl radicals and solvated electrons were available in solution in equivalent and higher

amounts than in water only. This asks the question of the mechanisms at stage and beside the negative/positive electron affinity hypothesis usually mentioned, we proposed, as for other nanomaterials, that interfacial water could play an essential role in radicals' production in solution when detonation H-ND are irradiated.

Acknowledgments

The authors would like to thank Stéphanie Droniou (Laboratoire de Chimie Physique, CNRS UMR 8000, Université Paris-Sud, Orsay, F-91405, France) for assistance during irradiation of the samples. Authors would like also to acknowledge Michel Schlegel (CEA, DEN, SEARS, Université Paris-Saclay) for complementary Raman characterization and Mohammed Sennour (Mines Paris Tech) for HR-TEM observations.

1. Introduction

Diamond nanoparticles, also named nanodiamonds (ND), were discovered long before nanomedicine becomes the vast and fast-growing research domain it is now [1]. Historically, the first man-made ND were obtained by detonation, a method that leads to quasi-monodisperse, quasi-spherical, 5 nm nanoparticles. Their small diameter and narrow size distribution make them ideal candidates for biological applications but if unmodified, they have a limited colloidal stability. Many other synthetic routes have been explored [2] giving birth to numerous diamond nanomaterials with different properties, but detonation synthesis provides the major source of ND.

Whatever the production method, purification steps are needed to get rid of metallic impurities and non-diamond structures. Oxidative treatments are the gold standard, resulting in mixed surface groups with carboxyl, carbonyl, hydroxyl and ether terminations. To obtain a more defined and controlled surface, several methods have been developed to obtain oxidized, hydrogenated, graphitized, halogenated or N-terminated ND and the surface can be further functionalized using linkers [3].

Obviously, the nature of ND terminations governs physico-chemical properties such as stability in solution or hydrophobicity but deeper impact has been revealed, for example on the electronic structure of diamond. Bolker et al. demonstrated that hydrogenated ND (H-ND) with diameter down to 4 nm, as hydrogenated bulk diamond, possess a negative electron affinity (NEA) i.e. their conduction band edge lies above the vacuum level [4]. If electrons are promoted from the valence to the conduction band, they can escape the diamond surface with a negligible energetic barrier, making H-ND a potential photoreductant. Surface groups also influence interactions with cells and toxicological characteristics. For instance, Woodhams et

al. showed different uptakes and toxicities for graphitized and oxidized ND in breast cancer cell lines [5]: despite a lower uptake, graphitized ND induce a higher level of oxidative stress.

But what makes ND exciting among the "bestiary" of nanomaterials developed for biology and medicine? First, ND powders are already produced at industrial scale at a low cost. Their core is chemically inert, whereas their surface chemistry allows a wide panel of functionalization, increasing their stability, modifying their properties as mentioned above, and paving the way for drug delivery [6, 7]. Crystallographic defects create color centers like NV, SiV or GeV that do not photobleach or blink as they are protected in the lattice, providing a promising alternative to quantum dots for bioimaging [8, 9]. As regards their toxicity, ND are considered as the most biocompatible among the carbonaceous nanomaterials [10, 11]. Indeed, carboxylated nanodiamonds were recently proposed as a negative control for nanogenotoxicity studies according to regulatory tests [12]. Besides drug delivery, bioimaging and biosensing, considered as the major bioapplications developed so far for ND [13], radiotherapy has to be added to the list since the pioneering work of Grall et al. [14]. These authors found that the incubation of radioresistant cancer cells with H-ND followed by irradiation (660 keV photons from ^{137}Cs) induced more cell death than H-ND or irradiation alone. This impairment was reproduced with three different cell lines. They also reported an increase in DNA damage 2h after irradiation, testifying of a higher level of oxidative stress at early time points. One possible explanation could be the production of reactive oxygen species by H-ND, which encourages us to conduct *in vitro* experiments.

Indeed, we recently investigated the hydroxyl radicals production by detonation ND under X-ray irradiation in solution [15]. In this previous work, we compared detonation ND differing only by their surface chemistry (H-ND and carboxylated-ND (Ox-ND)). Under non-

monochromatic 17.5 keV X-rays, only H-ND showed an overproduction of 40% of hydroxyl radicals in water, testifying for the importance of functionalization as underlined before. Interestingly, this phenomenon was independent from the commercial source of ND, proving that the key parameter was linked to the hydrogen termination. These first results lead us to the following questions: i) is the overproduction of hydroxyl radicals still present when higher energy photons are used? This could provide a more robust comparison with [14]; ii) is there any production of solvated electrons when H-ND are irradiated?

To answer these points, quantification of hydroxyl radicals after 1.3 MeV irradiation in the presence of H-ND or Ox-ND was achieved. We applied the same protocol as in [15], with coumarin as a specific $HO^{\bullet}$ scavenger. To quantify solvated electrons, we benefited from a new development of this protocol, the proof of concept being recently published with gold nanoparticles [16]. We thus got access to the production of hydroxyl radicals and solvated electrons, for keV photons, by two types of ND (hydrogenated and oxidized). These nanodiamonds were carefully characterized using complementary analytical tools that previously proved their efficacy to probe the diamond core (High Resolution Transmission Electronic Microscopy - HR-TEM [17] and Raman spectroscopy [18]), the surface chemistry (Fourier Transformed Infra-Red spectroscopy - FTIR [19], X-ray Photoelectron Spectroscopy - XPS [20]) and their colloidal properties in water (Dynamic Light Scattering - DLS).

2. Experimental section

2.1. Preparation of nanodiamonds

Detonation nanodiamonds (ND) were purchased from Plasmachem Company (Germany, G02 grade). Oxidized ND (Ox-ND) were produced by annealing under air for 1h30 at 550°C. Hydrogenated ND (H-ND) were obtained by plasma treatment using a home-made CVD

reactor [21]. Briefly, ND were deposited in a quartz tube and exposed to a H_2 microwave plasma (gas pressure: 12 mbar; gas flow:10 standard cubic centimeters per minute; power: 200 W) for 75 min.

Particles were then dispersed in ultrapure water (18.2 MΩ.cm) and sonicated (Heilscher UP400s, 300 W, 24 kHz) for 1h under cooling. Suspensions were then centrifuged for 40 min (2400 g) to remove aggregates. Final concentration was calculated by measuring the mass of residue after drying a calibrated volume of the initial suspension.

2.2. Characterization of nanodiamonds

Dynamic light scattering (DLS) and zeta potential measurements

Hydrodynamic diameters and zeta potentials were measured by dynamic and electrophoretic light scattering in DTS1070 cells (Malvern) with a Malvern NanoZS. Acquisitions were realized at 25°C with a 173° backscattered angle on diluted suspensions (0.5 $mg.mL^{-1}$) in ultrapure water (pH ≈ 6). For size measurements, we used a refractive index of 2.417. For zeta measurements, 150 V were applied (Smoluchowski equation). Size distributions result from the average of ca. 20 independent measurements, performed on the six, resp. two distinct suspensions for H-ND, resp. Ox-ND, used in this study.

Vibrational spectroscopies

FTIR spectra were recorded on a Vertex 7 spectrometer equipped with an ATR. 1 µL of a pellet of ND suspension was deposited and dried on the crystal. Spectra were recorded by accumulating 128 scans with a resolution of 4 cm^{-1}. ATR spectrum was recorded in the same conditions as a reference just before each experiment and was subtracted from the ND spectrum.

Micro-Raman measurements presented in this paper were performed at 325 nm, using a Renishaw InVia spectrometer. A UV-dedicated 40x (NA = 0.5) objective was used to focus the laser at the sample surface and collect the scattered light. To lower the incident power at the sample, the line mode of the spectrometer was used, giving power densities below 10 $\mu W/\mu m^2$. Only these weak irradiance conditions made it possible to correctly analyze these samples. Other experimental details may be found in Ref [18]. Supplementary measurements were also conducted at 532 nm.

High Resolution Transmission Electronic Microscopy

Observations were realized using a Tecnai HR-TEM (F20 FEI at 200kV) equipped with a Gatan Imaging Filter, corresponding to a high lateral resolution of 2.3 Å. Nanodiamonds from colloidal suspension were deposited on a 3 mm diameter copper grid covered with a holey carbon film by manual dip coating. Images were performed near Scherzer focalization (−63 nm) using a (1 k × 1 k) charge-coupled device camera.

X-ray Photoelectron Spectroscopy

40 µL of ND in stock aqueous suspension (1-2 $mg.mL^{-1}$) were deposited by drop-casting on a silicon substrate coated with a gold layer (100 nm) to ensure surface conductivity and prevent charging effects. High resolution X-ray photoelectron spectroscopy (XPS) spectra were acquired using a monochromatized Al $K\alpha$ anode (1486.6 eV) calibrated versus the Au $4f_{7/2}$ peak located at 84.0 eV. The spot size is 600 microns. The spectrometer was equipped with an EA 125 hemispherical analyzer. The pass energy was 20 eV, corresponding to an energy absolute resolution of 0.6 eV. The XPS data of core levels were corrected thanks to a Shirley-background subtraction.

2.3. Irradiation

Most of ND samples were prepared in coumarin solution with a final concentration of 0.5 mM (Sigma, >99 %, diluted in ultra-pure water). Some experiments were also performed with 2, 3 or 6 mM coumarin. Irradiations were performed with two facilities: a X-rays generator (Diffractis 583 Enraf Nonius, Mo cathode, non-monochromatic X-rays of 17.5 keV effective energy) and a panoramic ^{60}Co source (IL60PL Cis-Bio International). Dose rates, assessed by Fricke dosimetry, were 18 Gy.min^{-1} for X-rays and between 7 and 10 Gy.min^{-1} for γ-rays depending on the exact location of the sample on the irradiation table.

2.4. HPLC analysis

Coumarin oxidation products were analysed from non-oxidized coumarin using HPLC (Beckman 168) in reverse phase (Kromasil C18 5µm 250x4.6 mm) with a gradient between two elution buffers A (89% water, 10% methanol and 1% acetic acid) and B (89% methanol, 10% water and 1% acetic acid). After irradiation and removal of ND by NaCl addition (1% w:v) and centrifugation (18 000g during 5 minutes), the supernatants injected were submitted to the following gradient with a 0.8 mL min-1 flow rate: 0% B during 5 min, 0-30% B in 5 min, 30-50% B in 20 min, 50-100% B in 5 min. The absorbance was recorded at 280 nm.

2.5.Quantification of hydroxyl radicals

The detailed protocol was already described in [15, 22]. After irradiation (highest dose ~ 30 Gy for γ-rays and ~ 12 Gy for X-rays), NaCl solution (final concentration of 1% w:v) was added to induce aggregation and all samples were centrifuged (18 000 g, 5min) to remove ND before fluorescence reading. Fluorescence of 7-hydroxycoumarin present in the supernatant was quantified at ca 452 nm after 326 nm excitation (Synergy H1 microplate reader, Biotek). Data processing was thoroughly explained in [16].

2.6. Quantification of solvated electrons

As proposed in [16], we adapted the coumarin assay to quantify solvated electrons. Prior to irradiation, samples were degassed with a tailored gas mixture (N_2O 79%, O_2 21%, Air Liquide). Nitrous oxide scavenges electrons, leading to hydroxyl radicals in a stoichiometric manner according to:

$$e^-_{solv.} + N_2O + H_2O \rightarrow HO^\bullet + HO^- + N_2 \quad (1)$$

As a N_2O-saturated solution corresponds to 25 mM of dissolved N_2O at 1 atm and 25°C [23] and given the rate constant of this reaction ($k = 9.10^9$ $L.mol^{-1}.s^{-1}$ [24]), the pseudo-one order kinetics leads to an electron capture in a few ns. O_2 is also known as an electron scavenger and indeed its rate constant indicates a diffusion-limited process ($k = 1.9.10^{10}$ $L.mol^{-1}.s^{-1}$ [24]) but its lower solubility (0.2 mM at 1 atm and 25°C) leads to a slower capture (around 150 ns), meaning that all solvated electrons are transformed into hydroxyl radicals.

By comparing $HO^\bullet$ production under air and N_2O/O_2 atmospheres, electron production can be extracted.

3. Results

3.1. Characterization of nanodiamonds

This work aims to quantify hydroxyl radicals and solvated electrons produced by ND submitted to ionizing radiations. For such a purpose, two different surface treatments (microwave hydrogen plasma and air annealing) were used with the aim to prepare two different surface chemistries, namely hydrogenated and oxidized surfaces. These ND were first characterized in terms of their core, composition and surface chemistry to ensure the relevance of the comparison of their properties under irradiation.

HR-TEM pictures of both types of ND are given in Figure 1A and B for Ox-ND and H-ND, respectively. Individual particles exhibit nearly spherical shapes and primary diameters

ranging from 2 nm to 8 nm, a majority of particles having a mean size of 5 nm, which is expected for detonation nanodiamonds. We measured an interplane distance of 2.06 Å, characteristic of (111) diamond planes [25], testifying that the diamond core is preserved whatever the treatment for particles close to the mean size. For detonation ND, a core-shell structure is commonly assumed, with a crystalline diamond core of ca. 4 nm in diameter, surrounded by a ca. 0.7 nm thick more or less amorphous shell. This shell can be observed on our HR-TEM images, particularly for H-ND (see the arrow in Fig. 1B). Furthermore, we cannot exclude the presence of some graphitic structures in these hydrogen-treated samples, but difficult to clearly identify on these HR-TEM pictures because of a too strong agglomeration of particles. In comparison, oxidized ND tend to exhibit a smoother surface [26, 27].

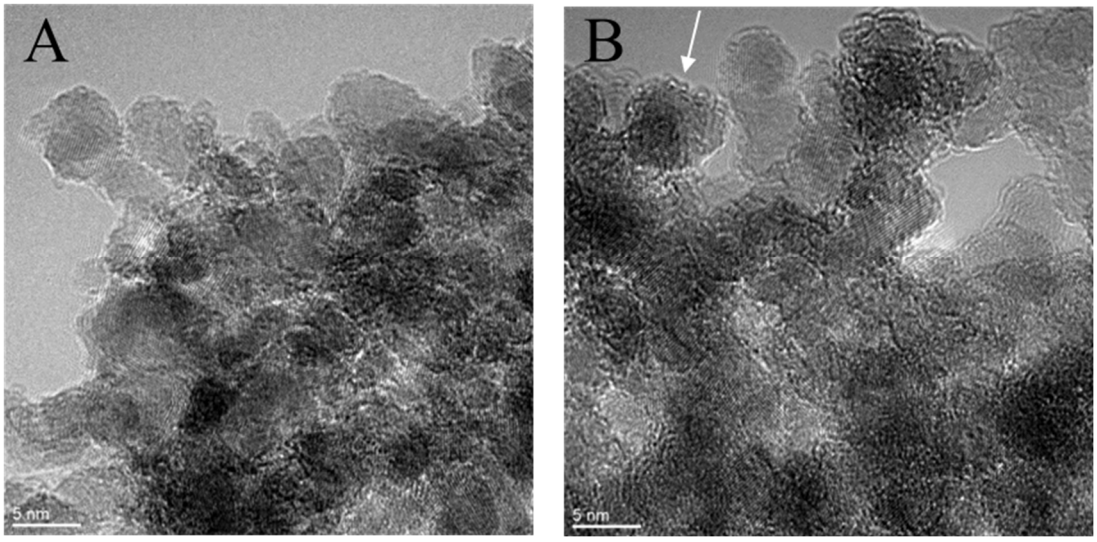

Figure 1: HR-TEM: images of Ox-ND (A) and H-ND (B). Scale bar represents 5 nm.

The same samples were subsequently analyzed by Raman spectroscopy, see Fig.2. Both spectra exhibited the expected asymmetric diamond Raman line at about 1327-1330 cm^{-1}, which obviously corresponds to the nanoparticle diamond core. On the other hand, the high frequency part of the spectra, or the so-called "G" line was sample dependent. It was observed at about 1640 and 1600 cm^{-1} for the oxidized and hydrogenated samples, respectively.

Another broad contribution was clearly detected at about 1400 cm^{-1} for the hydrogenated sample. Clearly, the 1600 and 1400 cm^{-1} contributions correspond to the expected frequencies of disordered graphite for this specific excitation wavelength (325 nm). A complete discussion of the 1640 cm^{-1} contribution falls out the scope of this paper [18 and Refs herein]. Supplementary analysis conducted at 532 nm gave exactly the same trends and conclusions. For both excitation wavelengths, note that only the use of very low power densities allowed the graphite detection. Thus, in agreement with previous studies [18], plasma hydrogenation seems to lead to a partial sample graphitization. However, particle surface graphitization only concerned the smallest particles, while biggest particles (>5 nm) were not affected [18]. It may be anticipated that this is still the case here, even if the hydrogenation conditions used in this study are not strictly similar to those used in Ref [18]. Here, Raman spectroscopy results tend to show that the surface chemistry of these particles is undoubtedly not as "binary" as the terms “hydrogenated” and “oxidized” may suggest.

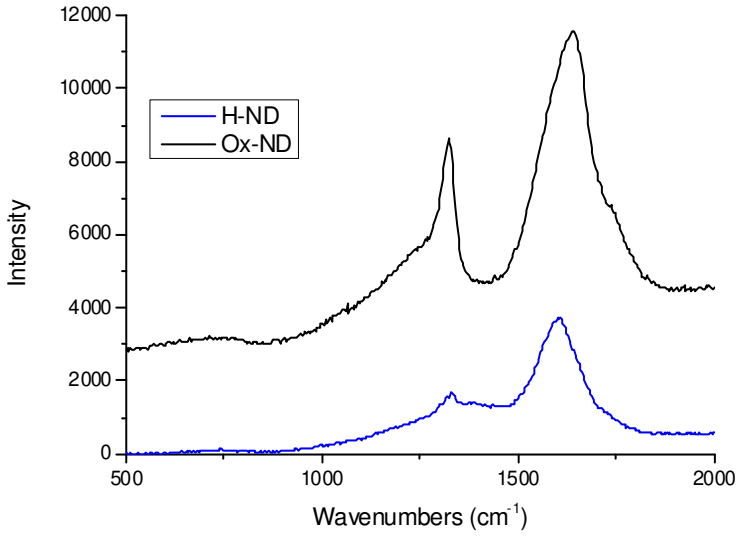

Figure 2: Raman spectra of Ox-ND and H-ND

Through X-ray photoelectron spectroscopy (XPS), atomic content was quantified for both ND using the C1s, O1s and N1s core levels (Figure 3). As expected, carbon is the overwhelming

component in both cases. Oxygen represents 16.5 at. % of all atoms in Ox-ND and is reduced down to 7.5 at. % in H-ND. This value is slightly higher than the usual 5% quantified on freshly H-ND. Remaining oxygen may come from adsorbed layers at the surface of NDs, as already reported in [28], as well as from a weak re-oxidation of the ND surface which cannot be exculded as H-ND have been suspended in water for several days prior to this XPS experiment. Finally, nitrogen represents less than 2 at. % for both treated ND. No metallic contamination from the sonicator (Ti), from the quartz tube (Si) or from the crucible used for the thermal treatment (Al) was detected (at the detection limit of XPS, ≈ 0.2-0.5 at. % [20]). Note that gold components visible on the survey spectrum correspond to the substrate on which ND were deposited for the analysis and allow an internal energy calibration.

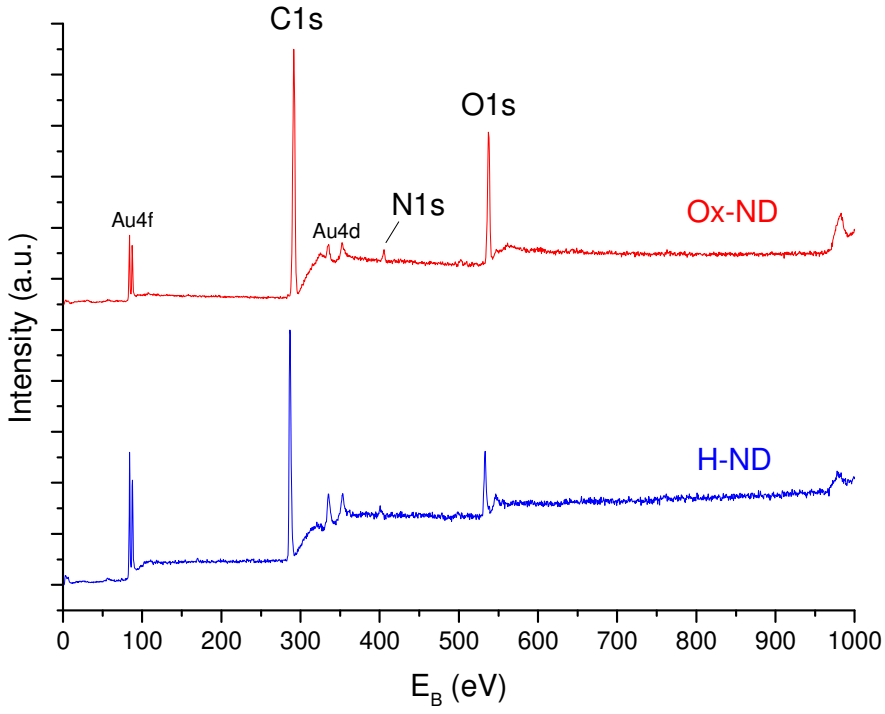

Figure 3: XPS survey spectra of Ox-ND (top, red) and H-ND (bottom, blue) deposited on a gold-coated silicon substrate.

Finally, as quantification of radicals was performed in solution, hydrodynamic diameters of H-ND and Ox-ND in water suspension were investigated by DLS. If we consider the distributions given in Figure 4A and B, plotted by the number of particles, it appears that both surface chemistries exhibit similar sizes: Ox-ND and H-ND have mean hydrodynamic diameters of 50 ± 8 and 48 ± 6 nm, respectively. Given the 5 nm primary particle size (Figure 1), it also reveals the formation of small clusters of a few particles in solution, even after sonication. Contrarily, Ox-ND and H-ND differ by their zeta potential of –55 mV and +40 mV respectively, which is a good indication of different functionalizations. These values are in agreement with our previous published data [15, 28].

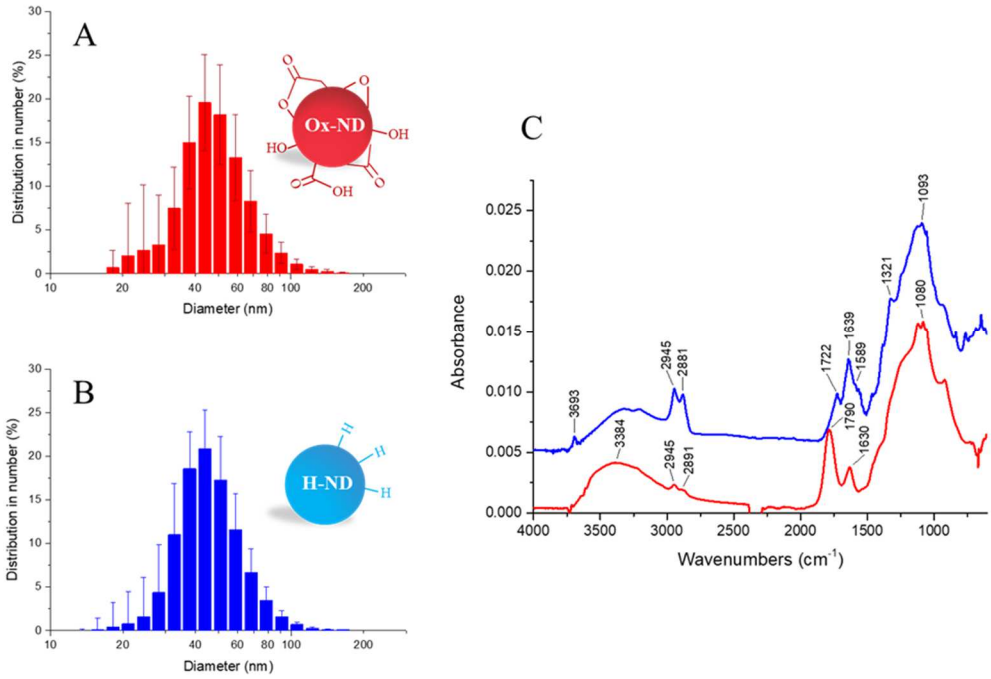

Figure 4: Characterization of the aqueous suspensions of ND. Left: Hydrodynamic size distribution in number according to DLS measurements for Ox-ND (A, top, red) and for H-ND (B, bottom, blue). These histograms represent data from all the independent batches used in this study for irradiation experiments (6 for H-ND and 2 for Ox-ND). Right: FTIR spectra of representative batches of Ox-ND (bottom, red) and H-ND (top, blue, an offset was added for clarity) (C).

To study in more details the two different sample surfaces, FTIR spectra of H-ND and Ox-ND were recorded after deposition of suspension droplets on an ATR crystal. They are given in Figure 4C. Ox-ND reveal strong C=O and C-O stretching bands, respectively located around 1790, 1080 and 920 cm^{-1}, associated with oxidized terminations at the ND surface such as carboxylic groups and cyclic ketones. At 1630 cm^{-1}, O-H bending band also testifies for the presence of water. Very small peaks at 2945 and 2891 cm^{-1} are still present for the oxidized particles though they represent the asymmetric and symmetric CH stretching modes, respectively. These stretching modes are much more significant in the case of H-ND with two maxima located at 2945 and 2881 cm^{-1}, indicating an efficient hydrogenation. For H-ND, contribution of C=O is weaker and down-shifted to 1730 cm^{-1}, revealing a different nature of CO groups, probably ketones and aldehydes. Also, hydration of samples sharpens the bending OH peaks, now found at 1637 cm^{-1}. Other line and/or apparent maxima are more difficult to comment as they fall in the frequency range where intrinsic diamond IR absorption, partially nitrogen-induced, is expected. Nevertheless, the very broad band with a strong contribution at 1090 cm^{-1} can be interpreted as the C-O-C stretching mode. This band is more intense than on spectrum of freshly prepared and dried H-ND (not shown), as already reported by Jirasek et al. [29]. This partial reoxidation of the H-ND, already observed in XPS analysis, may be assigned to their dispersion in water as suspensions were characterized several days after preparation, when irradiations were performed. However, infra-red signatures of Ox-ND (C=O stretching band) and H-ND (C-H stretching bands) are different enough to conclude expected functionalizations were achieved.

Thereby, according to this set of complementary techniques, Ox-ND and H-ND were effectively obtained, from the same nanodiamond core material. When dispersed in water,

they exhibit comparable hydrodynamic diameters. The influence of their surface chemistry is thus relevant to study.

3.2. Quantification of hydroxyl radicals in the MeV regime

In a previous study, we reported an overproduction of hydroxyl radicals when plasma-hydrogenated detonation nanodiamonds solutions are under irradiated at 17.5 keV. But, in radiotherapy, megavoltage photons are by far the most common: in conventional, intensity-modulated, tomographic or stereotactic treatments, specially-modified linear accelerators produce photons or electrons through 4-25 MV voltage. If photons of lower energies are still in use, superficial or orthovoltage units are restricted to superficial cancers and thus are not representative of the current modalities of treatments. That is why our first concern was to measure hydroxyl radicals in solution when ND were irradiated with megavoltage photons.

A panoramic ^{60}Co source delivering γ-rays of 1.17 and 1.3 MeV was utilized, it allows a large number of samples to be irradiated at the same time and has an adjustable dose rate. The extreme reactivity of hydroxyl radical, in addition to its small extinction absorption coefficient (ca 500 $L.mol^{-1}.s^{-1}$ at 230 nm [23]) precludes its direct detection and instead, a probe is needed. Our method is based on $HO^{\bullet}$ scavenging by coumarin [22]. $HO^{\bullet}$ attack results in several hydroxycoumarins among which 7-hydroxycoumarin is the only product to fluoresce. Its production is specific, that is to say no other reactive oxygen species can lead to 7-hydroxycoumarin, and is proportional to $HO^{\bullet}$ concentration. However, as nanoparticles are known to interfere with assay components and readout systems [30, 31], we first confirmed the accuracy of our radical quantification with OH-coumarin in the presence or absence of nanodiamonds. We performed chromatographic separation of the oxidized products obtained after coumarin was irradiated for doses up to 200 Gy. The comparison of HPLC profiles of

irradiated coumarin in absence or in presence of nanodiamonds (30 and 150 µg/mL) is given in Figure S1, and confirms the formation of all hydroxyl-coumarins in the same proportions with or without nanodiamonds. In addition, a dose increase was correlated with hydroxyl-coumarins increase in the same proportion (Figure S2 and S3). Therefore, we can confirm that our protocol is reliable in the presence of nanodiamonds. One should keep in mind that even the simplest radiolysis reactions involve a variety of reactive intermediates, which react and disappear at different rates. Competition between reactions takes place and the scavenging of $HO^{\bullet}$ by coumarin is no exception to the rule. Kinetics consideration is essential: given the rate constant of this reaction ($k=1.05\ 10^{10}$ $L.mol^{-1}\ s^{-1}$ [32]) and for example 0.5 mM concentration of coumarin, we can access the $HO^{\bullet}$ concentration at ca. 100 ns after the initial transfer of energy to water. It means that the quantification of such a reactive species strongly depends on the nature of the scavenger and its concentration: if fastest reactions occur, the quantification will be underestimated. That is why we decided to express our results as "apparent yield of formation of 7-hydroxycoumarin", noted G_{app}(7-hydroxycoumarin), "apparent yield of formation of hydroxyl radicals", noted $G_{app}(HO^{\bullet})$, which represents the quantity of $HO^{\bullet}$ available in solution for a given irradiation dose, or "available radicals reacting with coumarin", in relative values compared to water (enhancement factor). The values obtained for aqueous solutions of H-ND and Ox-ND under megavoltage photons fluxes are presented in Figure 5.

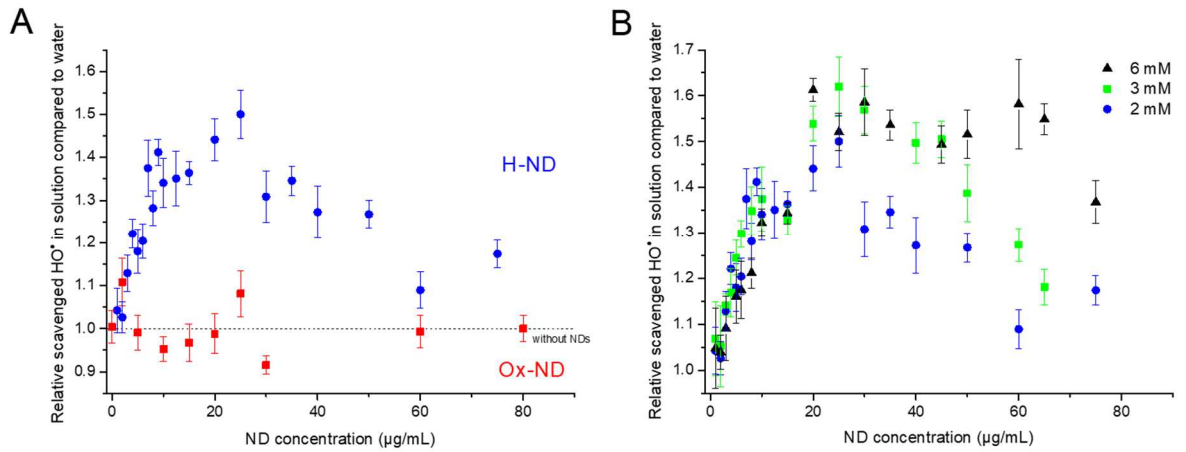

Figure 5: Available hydroxyl radicals in solution as a function of ND concentration when ND were irradiated with γ-rays. A: Comparison between H-ND (blue dots) and Ox-ND (red squares) suspensions. The dashed line represents the case of pure water (without ND). For H-ND, coumarin concentration was 2 mM and 3 independent experiments conducted with 2 different batches were averaged. For Ox-ND, coumarin concentration was 0.5 mM and 5 independent experiments conducted with 2 different batches were averaged. B: Influence of coumarin concentration for H-ND. Three different concentrations were tested: 2 mM (blue dots), 3 mM (green squares) and 6 mM (black triangles). At least two independent experiments were conducted in each case.

According to Figure 5A, Ox-ND do not lead to extra $HO^{\bullet}$ reacting with coumarin compared to water radiolysis when suspensions were irradiated with γ-rays. For most concentrations, the apparent yield of $HO^{\bullet}$ in solution is within 10% of the value for pure water. On the contrary, for H-ND, more $HO^{\bullet}$ are scavenged by coumarin than in water. For concentrations up to 10 $\mu g.mL^{-1}$, $G_{app}(HO^{\bullet})$ increases linearly with H-ND concentration, with a steep slope, that slows down from 10 to 25 $\mu g.mL^{-1}$. This results in an apparent maximal enhancement factor of 1.50 for 25 $\mu g.mL^{-1}$. For higher concentrations, a decrease in the apparent yield of $HO^{\bullet}$ is noticeable. This saturation is not attributable to a saturation of coumarin as curves representing [7-hydroxycoumarin]=f(dose) are linear in all the samples. This phenomenon could reflect the competitions mentioned above. To challenge this hypothesis, we performed similar experiments with higher coumarin concentrations (Figure 5B). Up to 10 $\mu g.mL^{-1}$, the three coumarin concentrations lead to the same relative scavenged hydroxyl radicals compared to water. For higher H-ND concentrations, the decrease in $G_{app}(HO^{\bullet})$ is shifted to

higher ND concentration and a plateau takes shape for 6 mM of coumarin. As mentioned before, it means that competitive processes are at stage and that above 20 µg.mL^{-1}, 7-hydroxycoumarin concentration don't reflect anymore the total HO$^{\bullet}$ concentration. In a nutshell, when MeV photons irradiate ND samples, the same trend as for keV photons is noteworthy [15]: surface chemistry has a major impact as only H-ND are able to generate more hydroxyl radicals in solution. We also demonstrated that hydroxyl radicals quantification does not depend on coumarin concentration up to H-ND concentration of 10 µg.mL^{-1}, which should lead to cautious interpretation.

If these oxidative radicals arise from secondary water radiolysis, they should go along with other radical and molecular species, namely solvated electrons ($e^-_{solv.}$), hydrogen atoms (H$^{\bullet}$), hydrogen peroxide (H_2O_2), …. We then focused on concomitant measurements of HO$^{\bullet}$ and $e^-_{solv.}$.

3.3.Quantification of solvated electrons

To extract the production of solvated electrons, 7-hydroxycoumarin must be titrated under two conditions: air and N_2O/O_2. As N_2O scavenges solvated electrons, leading to hydroxyl radicals (see Eq 1), the apparent yields of formation of species, available for coumarin scavenging, obey the following equation:

$$G_{app}(HO^{\bullet})_{N2O/O2} = G_{app}(HO^{\bullet})_{air} + G_{app}(e^-_{solv})_{air} \qquad (2)$$

By subtracting the curves $G_{app}(HO^{\bullet})_{N2O/O2}$ and $G_{app}(HO^{\bullet})_{air}$ as a function of ND concentration, we get access to the production of solvated electrons as a function of ND concentration. We performed these experiments under X-rays irradiation.

First, we submitted Ox-ND to irradiation under N_2O/O_2 atmosphere. Whatever the Ox-ND concentration, there was no difference in the relative amount of scavenged HO$^{\bullet}$ with or

without ND (data not shown), meaning that Ox-ND are spectator of the radiolysis process. Thereby, in line with what was reported in [15], under N_2O/O_2 atmosphere as under air, Ox-ND do not change the amount of available hydroxyl radicals or solvated electrons in solution.

For H-ND, quantification of 7-hydroxycoumarin was also performed after irradiation under N_2O/O_2 atmosphere, reflecting the total amount of hydroxyl radicals and solvated electrons. The corresponding results are presented in Figure 6A.

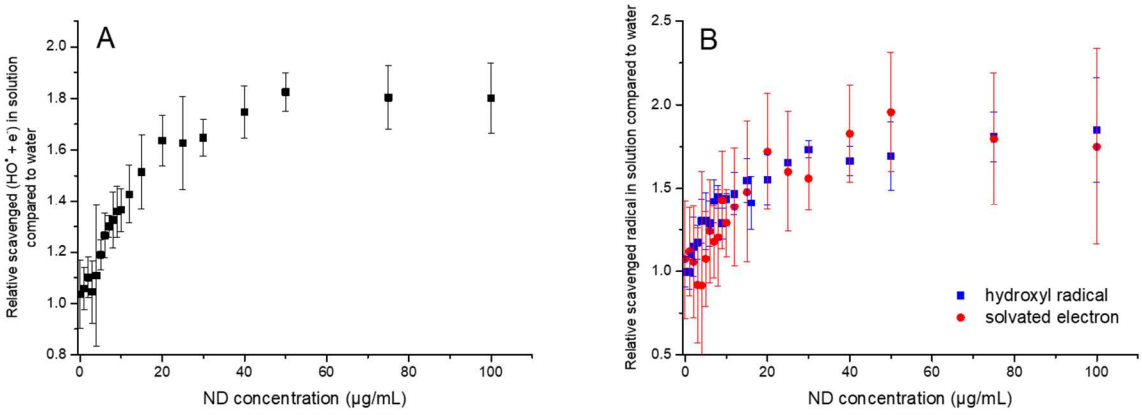

Figure 6: Quantification of solvated electrons. A**:** Total amount of hydroxyl radicals and solvated electrons compared to water, as a function of H-ND concentration for X-rays. These values were obtained after irradiation under N_2O/O_2. Two to eight independent experiments from 4 different H-ND batches were averaged per concentration. B: Relative quantification of hydroxyl radicals in solution (blue squares) and solvated electrons in solution (red dots) in the presence of H-ND compared to water only.

The apparent yield of total $HO^{\bullet}$ in solution increases with respect to H-ND concentration, with a linear relationship with a steep slope up to 10 $\mu g.mL^{-1}$ and a slower slope up to 20 $\mu g.mL^{-1}$. For higher concentrations a plateau is observed. Combining this curve and the one obtained under air for X-rays, the apparent yield of solvated electrons can be extracted (Figure 6B). For clarity's sake, G_{app}-values for solvated electrons and hydroxyl radicals in the presence of H-ND were compared to G-values in water and Fig 6B shows their ratios. To begin with, we have to highlight that H-ND, contrary to Ox-ND, lead to more solvated electrons available in solution when irradiated with keV photons than water. This establishes

the first experimental report of extra solvated electrons in the presence of 5 nm detonation H-NDs, available for subsequent reactions. For all tested H-ND concentrations, the G_{app}-values for e^-_{solv} are superior to the ones in water. Figure 6B also provides comparison between the two radical species we focused on in this study. Interestingly, apparent yields of solvated electrons and hydroxyl radicals are similar for the whole range of ND concentrations tested. As previously mentioned, only quantification from the first linear part of this curve is reliable. It means that an enhancement factor of 1.5 for solvated electrons and hydroxyl radicals is reachable when H-ND at low concentrations are irradiated with low doses of X-rays.

4. Discussion

This work was devoted to the measurement of hydroxyl radicals and solvated electrons produced when nanodiamonds are submitted to ionizing radiation. Given their redox potentials, these two species are of great interest to induce chemical reactions in a productive manner. Hydroxyl radicals are powerful oxidants that react at nearly diffusion rates with most organic substrates, making them ideal reactant for depollution or wastewater treatments [33-35]. Solvated electrons are able to induce reductive processes in a very efficient, waste-free, sustainable way, allowing unfavorable reactions to take place even in water [36].

We showed for the first time that irradiation of aqueous suspensions of 5 nm detonation H-ND by 1.3 MeV photons leads to higher concentrations of hydroxyl radicals in solution. This energy is close to the one used by Grall et al. (660 keV) to demonstrate an *in vitro* radiosensitization effect for H-ND [14] . As we evidenced similar productions of hydroxyl radicals for 17.5 keV X-rays and 1.3 MeV γ-rays, leading to an additional 50 % of radicals for H-ND concentration about 20 $\mu g.mL^{-1}$, we can expect an equivalent radical production at 660 keV. The dose range used for these measurements is worth noticing as ND were irradiated

from 0 to 30 Gy, which is in the same order of magnitude as radiotherapy treatments. A 10 Gy fraction of γ-rays provides ca. 3 µmol of $HO^{\bullet}$. In the presence of H-ND, the 1.5-fold increase could be significant and trigger cellular response leading to cell death.

We also focused on quantifying solvated electrons produced by the irradiation of ND suspensions and measured that equivalent amounts of hydroxyl radicals and solvated electrons are generated for keV photons. Interestingly, only H-ND increase radical concentrations while Ox-ND seem to be inert in the presence of ionizing radiations. We thus confirmed the marked difference in this process between two surface chemistries: oxidized and hydrogenated. The protocols used were tested for different sources of detonation ND with consistency and the artefactual overproduction due to potential high-Z contaminants was ruled out through XPS experiments (Figure 3). No metal was detected, meaning their content, if any, are under the XPS limit of detection i.e. lower than 0.2-0.5 at. % [20]. Such a weak concentration in ND, added to the low concentration of ND in the irradiated samples (sub 100 $\mu g.mL^{-1}$) is a strong argument in favor of a ND-involved production of hydroxyl radicals and solvated electrons.

If one excepts carbocatalysis, studies involving ND for radical production are scarce. Initial works were conducted in Hamers' team on bulk and thin films of hydrogenated [37] and aminated [38] diamond. Under UV illumination, photoemission of solvated electrons in water was probed directly by transient absorption measurements and indirectly via reduction of N_2 into NH_3 [37] or CO_2 into CO [39]. These authors underlined that emission of electrons depends critically on diamond surface termination as only substrates with NEA present an energy band diagram that favors electron escape. The transposition to ND proved to be more demanding. To our best knowledge, only highly crystalline 125 nm H-ND produced from natural diamond were able to initiate selective photochemical reduction of CO_2 [40] and attempts using detonation H-ND dispersed in water were not successful [40, 41]. When an electron is emitted from diamond, it must come along with an oxidation event to preserve

charge neutrality (hence the addition of a sacrificial electron donor to the ND suspension as in [40]). According to the authors, detonation H-ND, with their less ordered surface, would be more prone to auto-oxidation, then preventing a facile electron emission.

In the experimental conditions reported in the present paper, detonation H-ND do contribute to an overproduction of solvated electrons and hydroxyl radicals in solution. This could raise the question of their *in-situ* modification. Infrared spectroscopy as well as DLS and zeta measurements were then performed on irradiated H-ND suspensions (1000 Gy), which did not exhibit any obvious functionalization or colloidal alteration, even if these preliminary analyses would be advantageously completed by more sophisticated techniques. Still, the possible causes of such an overproduction merit further discussion.

Two main hypotheses could be proposed: either electrons are indeed emitted from ND and energetic enough to generate secondary radiolysis and/or this overproduction relies on interfacial processes. In the first case, the difference between H-ND and Ox-ND can be rationalized through their different surface chemistry, i. e. hydrogen terminations and graphitic structures for hydrogen plasma treated ND versus oxidised terminations for Ox-ND. But, as in the previously cited papers, detonation H-ND used in this study do not present the high crystalline perfection potentially required for photocatalysis. Moreover, the question of the oxidation by the valence-band holes remains. We did not add any sacrificial donor in our experiments but some radiolytic species formed by water radiolysis might play that role, probably helped by the graphitic carbon shell surrounding our H-ND as suggested by HR-TEM and detected in Raman [42, 43]. The second hypothesis is related to the key role water molecules at the nanoparticle interface could play in the radical production. A body of experimental data obtained on gold nanoparticles leads us to reconsider the traditional vision of the physical step, that is to say the increased absorption of photons by gold inducing

Compton or photoelectric effect to eject electrons, governing this phenomenon and to propose that the organization of water around gold NP favors its radiolytic dissociation [16]. For ND as well, considering the mass energy absorption coefficients of carbon and water, no drastic increase in energy deposit is expected in ND aqueous suspensions, be it for keV or MeV irradiation. But the interaction of water molecules around ND with different functionalizations has been more documented [44]. For example, ND powders annealed in air, nitrogen or hydrogen present different amounts of adsorbed water [45] and water molecules adsorb at lower vapor pressure on H-ND than on Ox-ND, leading to higher amount of water on H-ND despite their hydrophobicity [28, 46]. More recently, combining infrared, Raman and X-ray absorption spectroscopies, Petit et al. revealed different structures of water molecules surrounding ND when the surface chemistry is varied [47]. In particular, water hydrogen bonding network was found to be different in aqueous dispersions of detonation H-ND compared to Ox-ND, leading to a long-range disordering of water molecules and electron transfer in the H-ND hydration shell was proposed. So a difference in water arrangement could also be responsible for the different behaviors of H-ND and Ox-ND under irradiation.

Given our indirect measurement, we cannot rule out any of these two hypothesis and more work is needed to decipher the mechanisms at stage. A thorough characterization of the surface state of ND after irradiation could be informative as it could possibly reveal oxidation patterns. Finally, these experimental data would be advantageously supported by numerical simulations to investigate the electronic properties of water molecules in close interaction with H-ND.

5. Conclusion

With well-characterized nanomaterials and a robust methodology, we significantly improved our knowledge of the radical species produced in water in the presence of detonation H-ND and Ox-ND submitted to ionizing radiations. We revealed that high-energy photons, such as those at stage in radiotherapy, led to at least a 1.5-fold increase in hydroxyl radicals in solution for low irradiation doses and low ND concentrations. To the best of our knowledge, this is also the first time that solvated electrons in solution were quantified in the presence of detonation H-ND. We highlighted how surface chemistry is essential in such systems. This work paved the way of a better understanding of radiosensitization processes, through the description of the physico-chemical step, which could be seen as a bridge between the initial light-matter interaction and the biological damages but more generally speaking, of catalytic processes involving ND and their interfaces.

References

[1] N. Nunn, M. Torelli, G. McGuire, O. Shenderova, Nanodiamond: A high impact nanomaterial, Current Opinion in Solid State and Materials Science 21(1) (2017) 1-9.

[2] O. Shenderova, N. Nunn, Production and purification of nanodiamonds, in: J.-C. Arnault (Ed.), Nanodiamonds : Advanced Material Analysis, Properties and Applications, Elsevier2017, pp. 25-56.

[3] A. Krueger, Current issues and challenges in surface chemistry of nanodiamonds in: J.-C. Arnault (Ed.), Nanodiamonds : Advanced Material Analysis, Properties and Applications, Elsevier 2017, pp. 183-242.

[4] A. Bolker, C. Saguy, R. Kalish, Transfer doping of single isolated nanodiamonds, studied by scanning probe microscopy techniques, Nanotechnology 25(38) (2014) 385702.

[5] B. Woodhams, L. Ansel-Bollepalli, J. Surmacki, H. Knowles, L. Maggini, M. de Volder, M. Atature, S. Bohndiek, Graphitic and oxidised high pressure high temperature (HPHT) nanodiamonds induce differential biological responses in breast cancer cell lines, Nanoscale 10(25) (2018) 12169-12179.

[6] D. Ho, A. Zarrinpar, E.K. Chow, Diamonds, Digital Health, and Drug Development: Optimizing Combinatorial Nanomedicine, ACS Nano 10(10) (2016) 9087-9092.

[7] K. Turcheniuk, V.N. Mochalin, Biomedical applications of nanodiamond (Review), Nanotechnology 28(25) (2017) 252001.

[8] S.R. Hemelaar, P. de Boer, M. Chipaux, W. Zuidema, T. Hamoh, F.P. Martinez, A. Nagl, J.P. Hoogenboom, B.N.G. Giepmans, R. Schirhagl, Nanodiamonds as multi-purpose labels for microscopy, Sci Rep 7(1) (2017) 720.

[9] O.A. Shenderova, G.E. McGuire, Science and engineering of nanodiamond particle surfaces for biological applications (Review), Biointerphases 10(3) (2015) 030802.

[10] M. Chipaux, K.J. van der Laan, S.R. Hemelaar, M. Hasani, T. Zheng, R. Schirhagl, Nanodiamonds and Their Applications in Cells, Small 14(24) (2018) e1704263.

[11] K. van der Laan, M. Hasani, T. Zheng, R. Schirhagl, Nanodiamonds for In Vivo Applications, Small 14(19) (2018) e1703838.

[12] H. Moche, V. Paget, D. Chevalier, E. Lorge, N. Claude, H.A. Girard, J.C. Arnault, S. Chevillard, F. Nesslany, Carboxylated nanodiamonds can be used as negative reference in in vitro nanogenotoxicity studies, J Appl Toxicol 37(8) (2017) 954-961.

[13] X. Chen, W. Zhang, Diamond nanostructures for drug delivery, bioimaging, and biosensing, Chem Soc Rev 46(3) (2017) 734-760.

[14] R. Grall, H. Girard, L. Saad, T. Petit, C. Gesset, M. Combis-Schlumberger, V. Paget, J. Delic, J.C. Arnault, S. Chevillard, Impairing the radioresistance of cancer cells by hydrogenated nanodiamonds, Biomaterials 61 (2015) 290-8.

[15] M. Kurzyp, H.A. Girard, Y. Cheref, E. Brun, C. Sicard-Roselli, S. Saada, J.C. Arnault, Hydroxyl radical production induced by plasma hydrogenated nanodiamonds under X-ray irradiation, Chem Commun (Camb) 53(7) (2017) 1237-1240.

[16] M. Gilles, E. Brun, C. Sicard-Roselli, Quantification of hydroxyl radicals and solvated electrons produced by irradiated gold nanoparticles suggests a crucial role of interfacial water, J Colloid Interface Sci 525 (2018) 31-38.

[17] S. Turner, O. Shenderova, F. Da Pieve, Y. Lu, E. Yücelen, J. Verbeeck, D. Lamoen, G. Van Tendeloo, Aberration-corrected microscopy and spectroscopy analysis of pristine, nitrogen containing detonation nanodiamond, Physica Status Solidi A 210(10) (2013) 1976-1984.

[18] M. Mermoux, S. Chang, H.A. Girard, J.C. Arnault, Raman spectroscopy study of detonation nanodiamond, Diamond and Related Materials 87 (2018) 248-260.

[19] T. Petit, L. Puskar, FTIR spectroscopy of nanodiamonds: Methods and interpretation, Diamond and Related Materials 89 (2018) 52-66.

[20] J.C. Arnault, X-ray Photoemission Spectroscopy applied to nanodiamonds: From surface chemistry to in situ reactivity, Diamond and Related Materials 84 (2018) 157-168.

[21] H.A. Girard, J.C. Arnault, S. Perruchas, S. Saada, T. Gacoin, J.-P. Boilot, P. Bergonzo, Hydrogenation of nanodiamonds using MPCVD: A new route toward organic functionalization, Diamond and Related Materials 19(7-9) (2010) 1117-1123.

[22] C. Sicard-Roselli, E. Brun, M. Gilles, G. Baldacchino, C. Kelsey, H. McQuaid, C. Polin, N. Wardlow, F. Currell, A new mechanism for hydroxyl radical production in irradiated nanoparticle solutions, Small 10(16) (2014) 3338-46.

[23] J.W.T. Spinks, R.J. Woods, Introduction to radiation chemistry, third ed., Wiley, New-York, 1990.

[24] G.V. Buxton, C.L. Greenstock, W.P. Helman, A.B. Ross, Critical-Review of Rate Constants for Reactions of Hydrated Electrons, Hydrogen-Atoms and Hydroxyl Radicals in Aqueous-Solution, J Phys Chem Ref Data 17(2) (1988) 513-886.

[25] T. Petit, J.C. Arnault, H.A. Girard, M. Sennour, P. Bergonzo, Early stages of surface graphitization on nanodiamond probed by x-ray photoelectron spectroscopy, Physical Review B 84 (2011) 233407

[26] E. Nehlig, S. Garcia-Argote, S. Feuillastre, M. Moskura, T. Charpentier, M. Schleguel, H.A. Girard, J.C. Arnault, G. Pieters, Using hydrogen isotope incorporation as a tool to unravel the surfaces of hydrogen-treated nanodiamonds, Nanoscale 11(16) (2019) 8027-8036.

[27] S. Osswald, S. Yushin, V.N. Mochalin, S.O. Kucheyev, Y. Gogotsi, Control of sp2/sp3 Carbon Ratio and Surface Chemistry of Nanodiamond Powders by Selective Oxidation in Air, Journal of the American Chemical Society 128(35) (2006) 11635-11642.

[28] T. Petit, H.A. Girard, A. Trouve, I. Batonneau-Gener, P. Bergonzo, J.C. Arnault, Surface transfer doping can mediate both colloidal stability and self-assembly of nanodiamonds, Nanoscale 5(19) (2013) 8958-62.

[29] V. Jirasek, S. Stehlik, P. Stenclova, A. Artemenko, B. Rezek, A. Kromka, Hydroxylation and self-assembly of colloidal hydrogenated nanodiamonds by aqeous oxygen radicals from atmospheric pressure plasma jet, RSC Advances 8 (2018) 37681-37692.

[30] R.M. Crist, J.H. Grossman, A.K. Patri, S.T. Stern, M.A. Dobrovolskaia, P.P. Adiseshaiah, J.D. Clogston, S.E. McNeil, Common pitfalls in nanotechnology: lessons learned from NCI's Nanotechnology Characterization Laboratory, Integr Biol (Camb) 5(1) (2013) 66-73.

[31] J. Tournebize, A. Sapin-Minet, G. Bartosz, P. Leroy, A. Boudier, Pitfalls of assays devoted to evaluation of oxidative stress induced by inorganic nanoparticles, Talanta 116 (2013) 753-63.

[32] G. Louit, S. Foley, J. Cabillic, H. Coffigny, F. Taran, A. Valleix, J.P. Renault, S. Pin, The reaction of coumarin with the OH radical revisited: hydroxylation product analysis determined by fluorescence and chromatography, Radiation Physics and Chemistry 72(2–3) (2005) 119-124.

[33] M. Cheng, G.M. Zeng, D.L. Huang, C. Lai, P. Xu, C. Zhang, Y. Liu, Hydroxyl radicals based advanced oxidation processes (AOPs) for remediation of soils contaminated with organic compounds: A review, Chem. Eng. J. 284 (2016) 582-598.

[34] S. Gligorovski, R. Strekowski, S. Barbati, D. Vione, Environmental Implications of Hydroxyl Radicals (center dot OH), Chem. Rev. 115(24) (2015) 13051-13092.

[35] J.L. Wang, L.J. Xu, Advanced Oxidation Processes for Wastewater Treatment: Formation of Hydroxyl Radical and Application, Crit. Rev. Environ. Sci. Technol. 42(3) (2012) 251-325.

[36] S.Y. Yang, Y.T. Zhang, D. Zheng, Advanced Reduction Processes: A Novel Technology for Water Treatment, Prog. Chem. 28(6) (2016) 934-941.

[37] D. Zhu, L. Zhang, R.E. Ruther, R.J. Hamers, Photo-illuminated diamond as a solid-state source of solvated electrons in water for nitrogen reduction, Nat Mater 12(9) (2013) 836-41.

[38] D. Zhu, J.A. Bandy, S. Li, R.J. Hamers, Amino-terminated diamond surfaces: Photoelectron emission and photocatalytic properties, Surface Science 650 (2016) 295-301.

[39] L. Zhang, D. Zhu, G.M. Nathanson, R.J. Hamers, Selective photoelectrochemical reduction of aqueous CO(2) to CO by solvated electrons, Angew Chem Int Ed Engl 53(37) (2014) 9746-50.

[40] L. Zhang, R.J. Hamers, Photocatalytic reduction of CO_2 to CO by diamond nanoparticles, Diamond and Related Materials 78 (2017) 24-30.

[41] R.J. Hamers, J.A. Bandy, D. Zhu, L. Zhang, Photoemission from diamond films and substrates into water: dynamics of solvated electrons and implications for diamond photoelectrochemistry, Faraday Discuss 172 (2014) 397-411.

[42] A.S. Jalilov, C.H. Zhang, E.L.G. Samuel, W.K.A. Sikkema, G. Wu, V. Berka, T.A. Kent, A.L. Tsai, J.M. Tour, Mechanistic Study of the Conversion of Superoxide to Oxygen and Hydrogen Peroxide in Carbon Nanoparticles, ACS Appl. Mater. Interfaces 8(24) (2016) 15086-15092.

[43] E.L.G. Samuel, D.C. Marcano, V. Berka, B.R. Bitner, G. Wu, A. Potter, R.H. Fabian, R.G. Pautler, T.A. Kent, A.L. Tsai, J.M. Tour, Highly efficient conversion of superoxide to oxygen using hydrophilic carbon clusters, Proc. Natl. Acad. Sci. U. S. A. 112(8) (2015) 2343-2348.

[44] T. Petit, Interactions with solvent in: J.-C. Arnault (Ed.), Nanodiamonds : Advanced Material Analysis, Properties and Applications, Elsevier2017, pp. 301-321.

[45] S.F. Ji, T.L. Jiang, K. Xu, S.B. Li, FTIR study of the adsorption of water on ultradispersed diamond powder surface, Appl. Surf. Sci. 133(4) (1998) 231-238.

[46] S. Stehlik, T. Glatzel, V. Pichot, R. Pawlak, E. Meyer, D. Spitzer, B. Rezek, Water interaction with hydrogenated and oxidized detonation nanodiamonds - Microscopic and spectroscopic analysis, Diamond and Related Materials 63 (2016) 97-102.

[47] T. Petit, L. Puskar, T. Dolenko, S. Choudhury, E. Ritter, S. Burikov, K. Laptinskiy, Q. Brzustowski, U. Schade, H. Yuzawa, M. Nagasaka, N. Kosugi, M. Kurzyp, A. Venerosy, H. Girard, J.C. Arnault, E. Osawa, N. Nunn, O. Shenderova, E.F. Aziz, Unusual Water Hydrogen Bond Network around Hydrogenated Nanodiamonds, Journal of Physical Chemistry C 121 (2017) 5185-5194.